Supporting Information:

N-functionalized MXenes: Ultrahigh carrier mobility and multifunctional properties

Yangfan Shao[1,2], Fang Zhang[2], Xingqiang Shi [2,*], and Hui Pan[1,*]

[1] *Institute of Applied Physics and Materials Engineering, University of Macau, Macau SAR, China*

[2]*Department of Physics, Southern University of Science and Technology, Shenzhen 518055, China*

*E-mail: huipan@umac.mo (H.P.); shixq@sustc.edu.cn (X.S.);

Tel: (853)88224427; Fax: (853)88222426

Table S1. Calculated formation energies of 2D M_2CN_2 and M_2CH_2 (M = Nb and Ta).

System	E_f
Nb_2CN_2	-3.48
Ta_2CN_2	-4.18
Nb_2CH_2	-2.12
Ta_2CH_2	-1.92

Table S2. Calculated effective mass (m^*), deformation potential constant (E), 2D elastic modulus (C), and carrier mobility (μ) of Nb_2CN_2 at ε = 4% and Ta_2CN_2 at ε =

5%.

		m^*_z/m_0	m^*_a/m_0	E_z	E_a	C_{z_2D}	C_{a_2D}	μ_{z_2D}	μ_{a_2D}
		Γ'-Z	Γ'-X	eV		Jm^{-2}		$10^5cm^2V^{-1}s^{-1}$	
Nb_2CN_2	e	0.047	0.086	2.76	5.62	1357	1660	11.93	1.92
4%	h	0.1	0.045	2.95	0.66			4.6	252
Ta_2CN_2	e	0.1	0.1	0.65	2.22	1743	2071	82.5	8.4
5%	h	0.12	0.08	1.61	1.68			11.21	18.35

Note: Carrier types 'e' and 'h' denote 'electron' and 'hole', respectively. The m^*_z and m^*_a are carrier effective masses along zigzag and armchair directions, respectively. m_0 is the free electron mass. E_z (E_a) and C_{z_2D} (C_{a_2D}) are the deformation potential and 2D elastic modulus along the zigzag (armchair) directions, respectively. Mobility is calculated with the temperature T at 300 K. The vacuum level was set to zero for reference.

Table S3. Calculated effective mass (m^*) of Nb_2CN_2 and Ta_2CN_2

	Nb_2CN_2 (Γ-M)		Ta_2CN_2 (Γ-M)	
	m^*/m_0 (electron)	m^*/m_0 (hole)	m^*/m_0 (electron)	m^*/m_0 (hole)
PBE	0.12	0.10	0.09	0.09
HSE	0.13	0.10	0.10	0.10

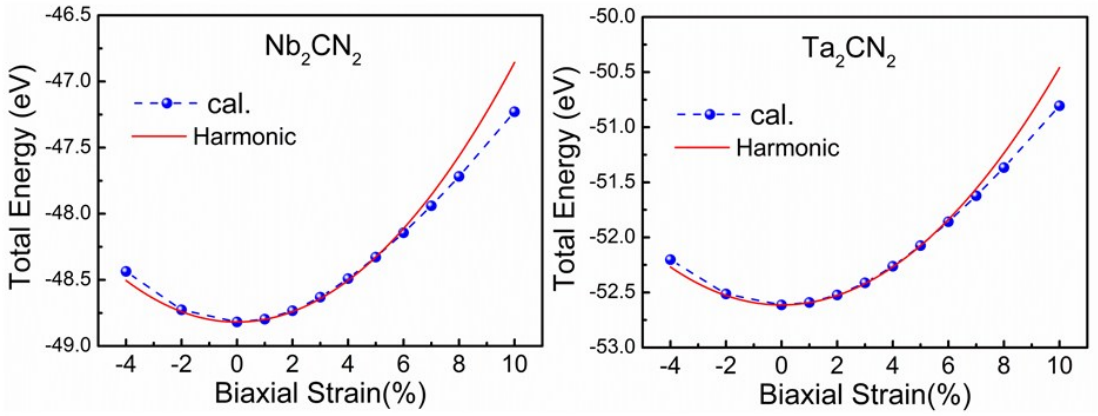

Fig. S1 Variation in the total energy of M_2CN_2 (M = Nb and Ta) under various biaxial strains shown by the dashed curve with large blue dots indicating the calculated data points. The harmonic part is fitted to a parabola presented by a red-solid curve.

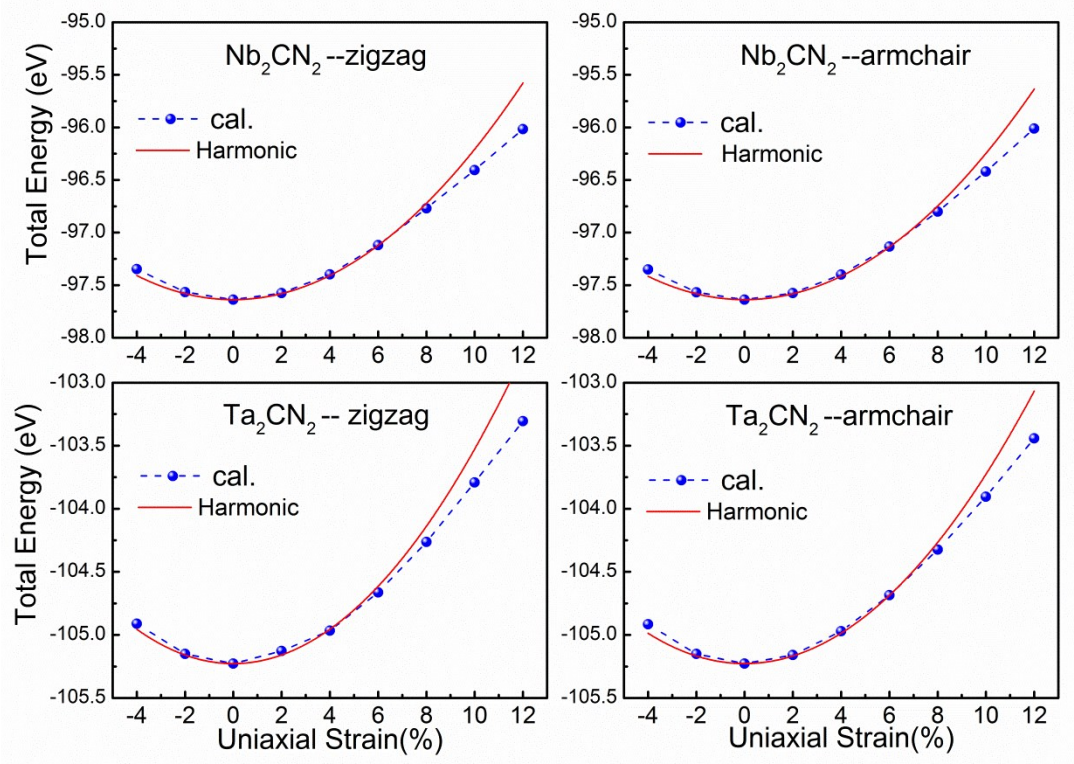

Fig. S2 Variation in the total energy of M_2CN_2 (M = Nb and Ta) under various zigzag and armchair shown by the dashed curve with large blue dots indicating the calculated data points. The harmonic part is fitted to a parabola presented by a red-solid curve.

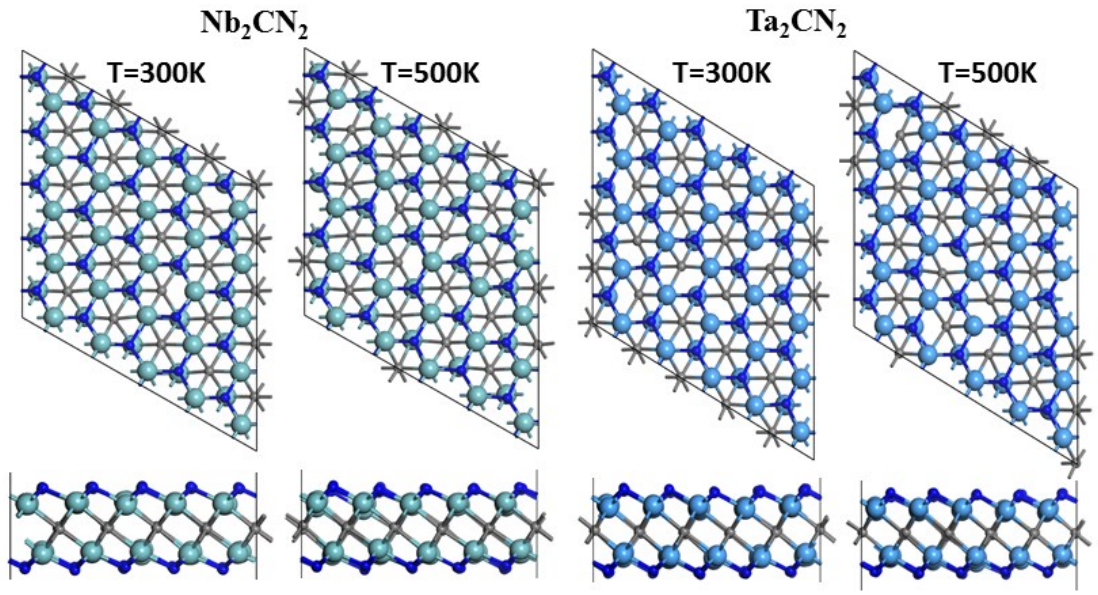

Fig. S3 Snapshots of atomic configurations of M_2CN_2 (M = Nb and Ta) at the end of AIMD simulations. The optimized atomic structures are displayed in the top and side views.

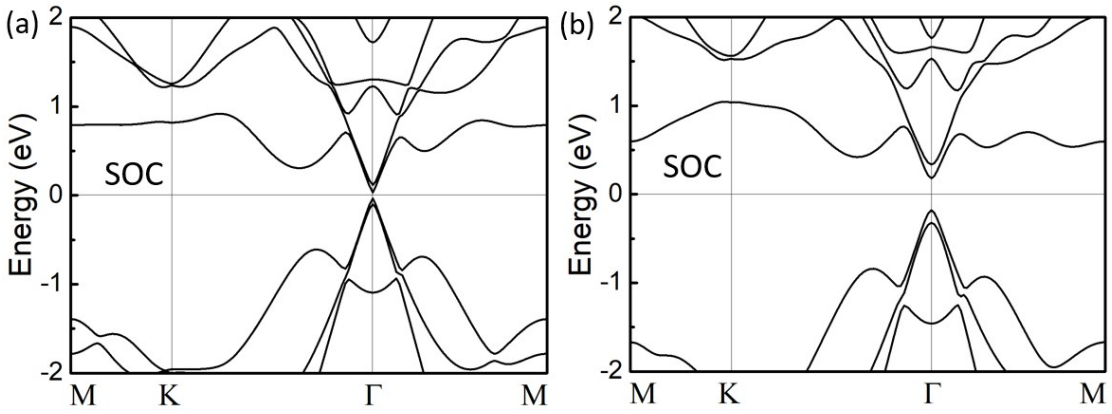

Fig. S4 Calculated PBE band structures of Nb_2CN_2 (a) and Ta_2CN_2 (b) with SOC.

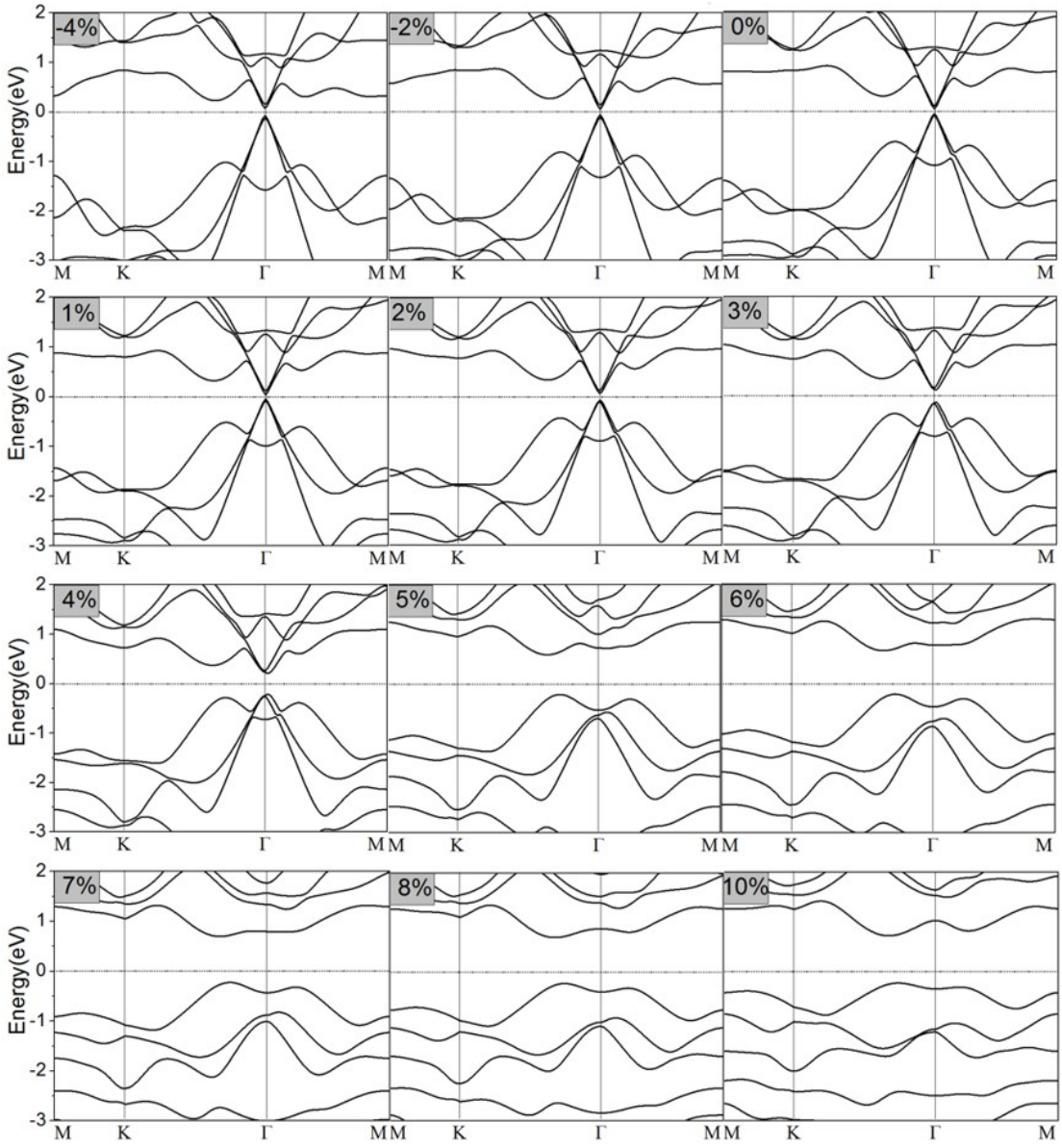

Fig. S5 The PBE band structures of Nb_2CN_2 under various biaxial strains along the high symmetry lines M-K-Γ-M of the Brillouin zone.

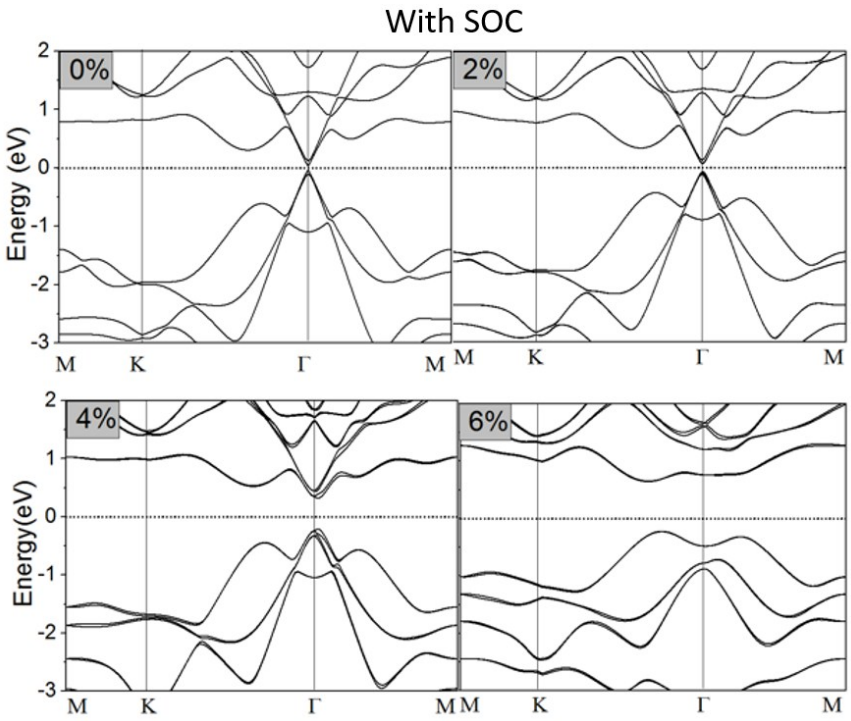

Fig. S6 The PBE band structures of Nb_2CN_2 with SOC under various biaxial strains along the high symmetry lines M-K-Γ-M of the Brillouin zone.

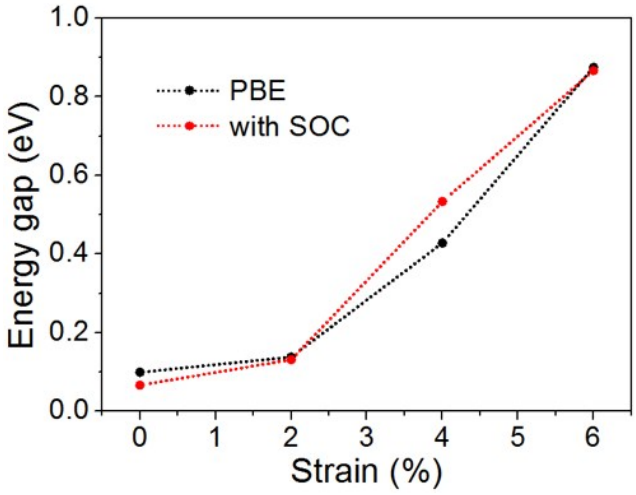

Fig. S7 The PBE band gap evolution of Nb_2CN_2 as a function of strain.

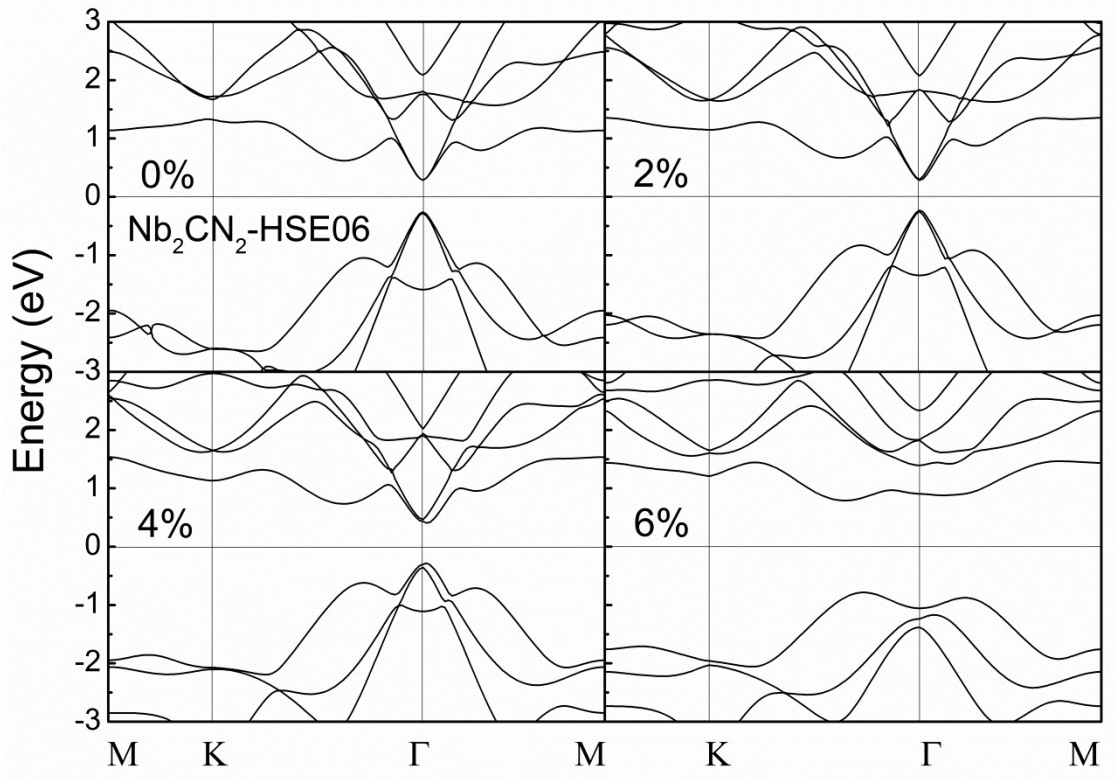

Fig. S8 Calculated HSE band structures of Nb_2CN_2 under various biaxial strains.

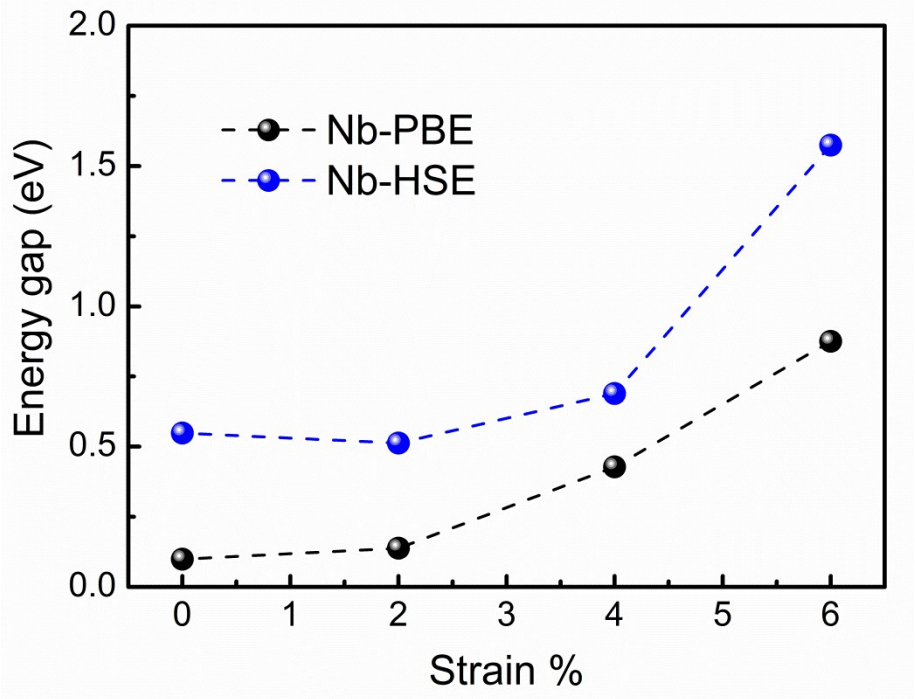

Fig. S9 The PBE/HSE band gap evolution of Nb_2CN_2 as a function of strain.

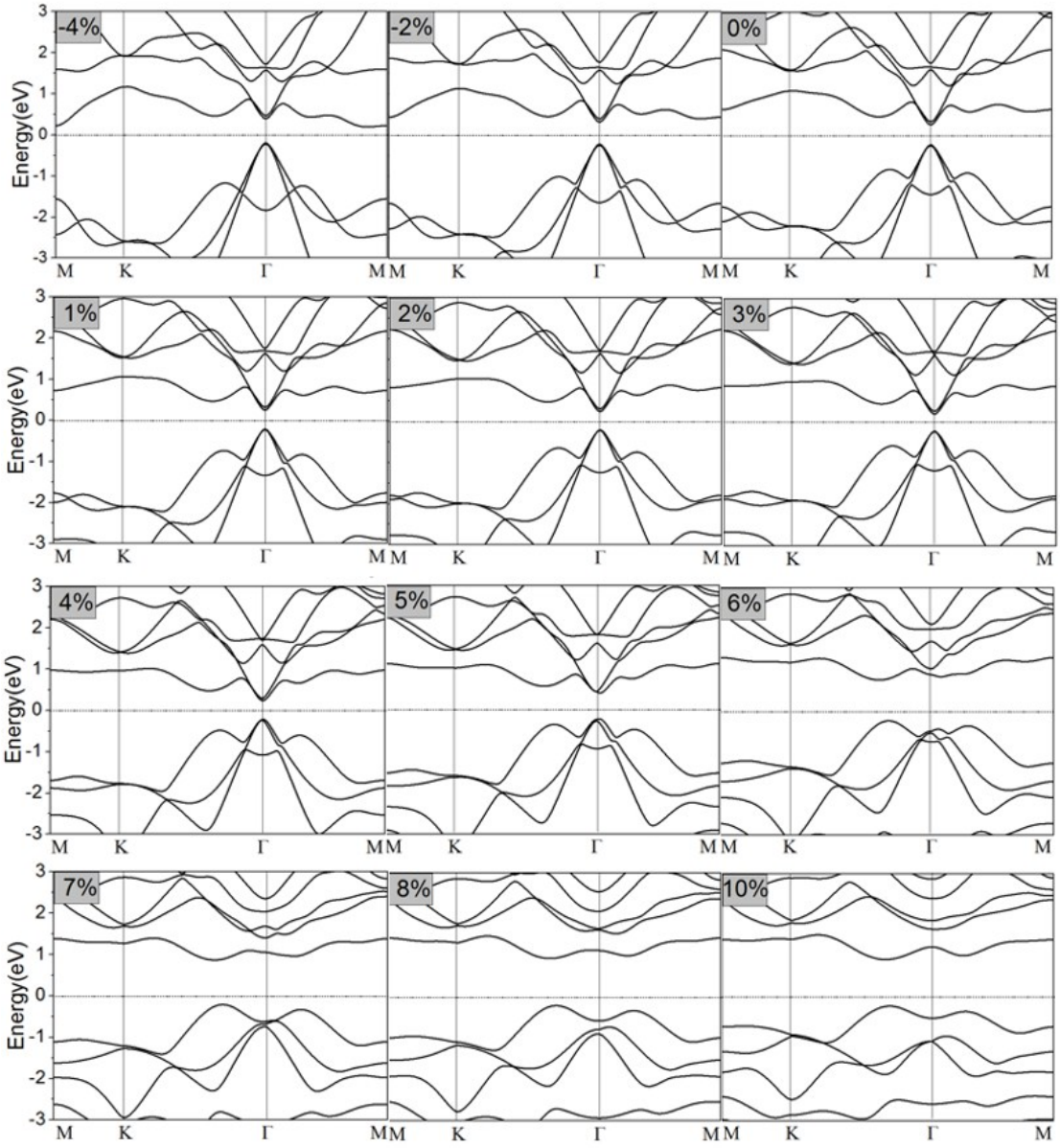

Fig. S10 The PBE band structures of Ta_2CN_2 under various biaxial strains along the high symmetry lines M-K-Γ-M of the Brillouin zone.

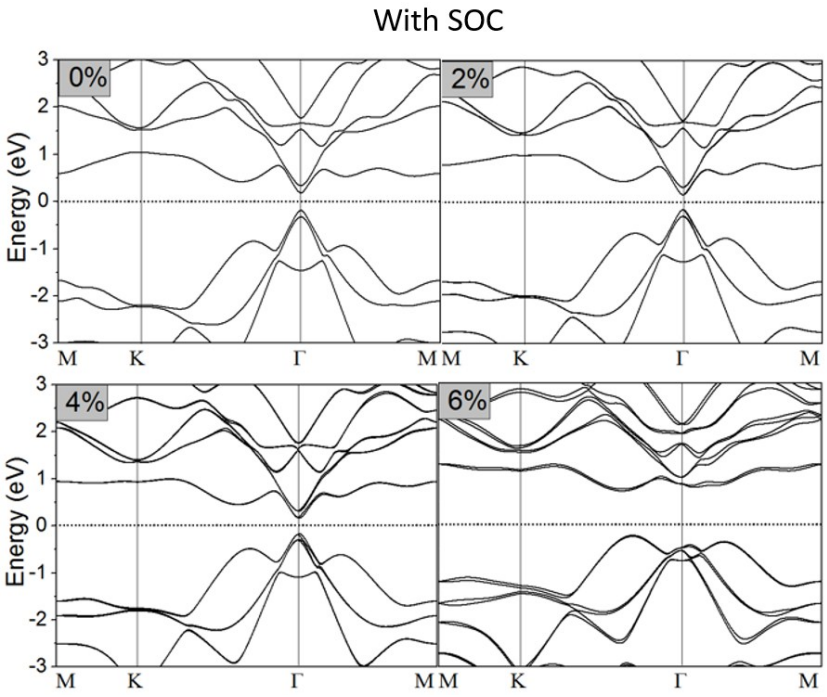

Fig. S11 The band structures of Ta_2CN_2 with SOC under various biaxial strains along the high symmetry lines M-K-Γ-M of the Brillouin zone.

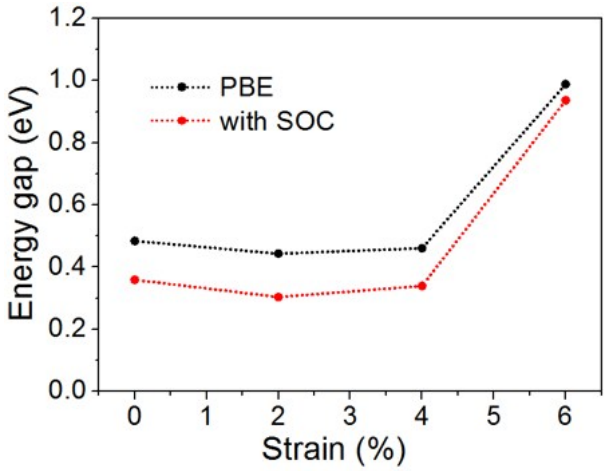

Fig. S12 The band gap evolution of Ta_2CN_2 as a function of strain.

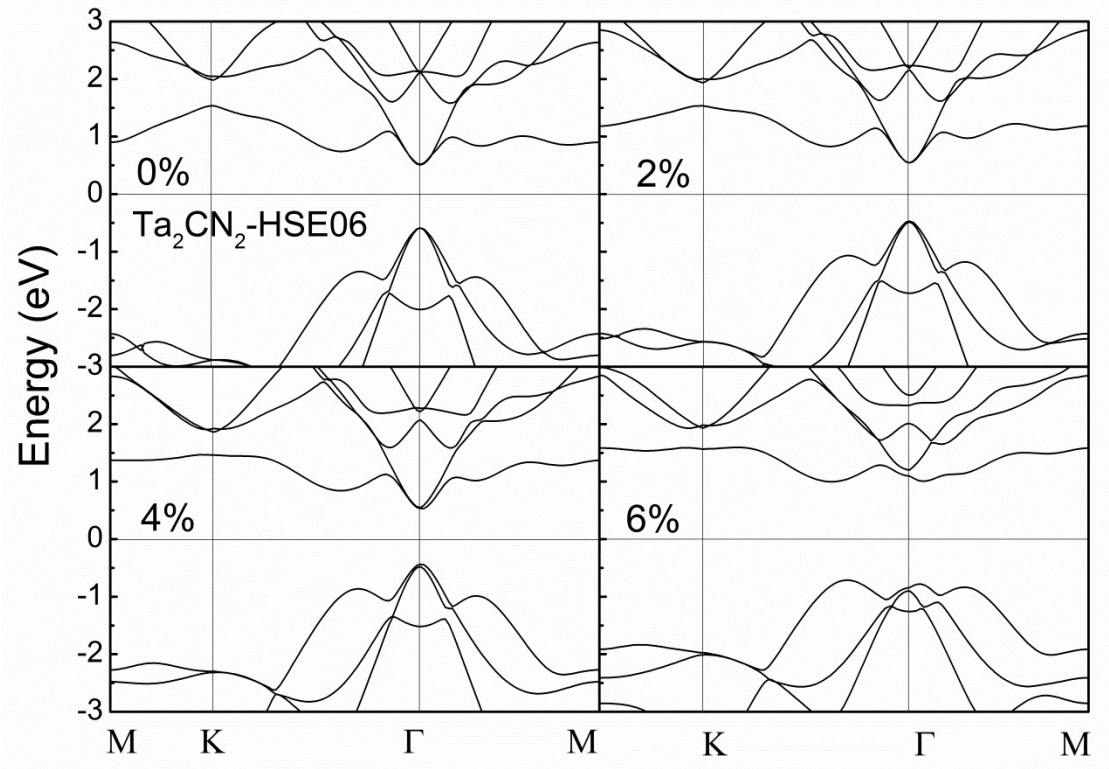

Fig. S13 Calculated HSE band structures of Ta_2CN_2 under various biaxial strains.

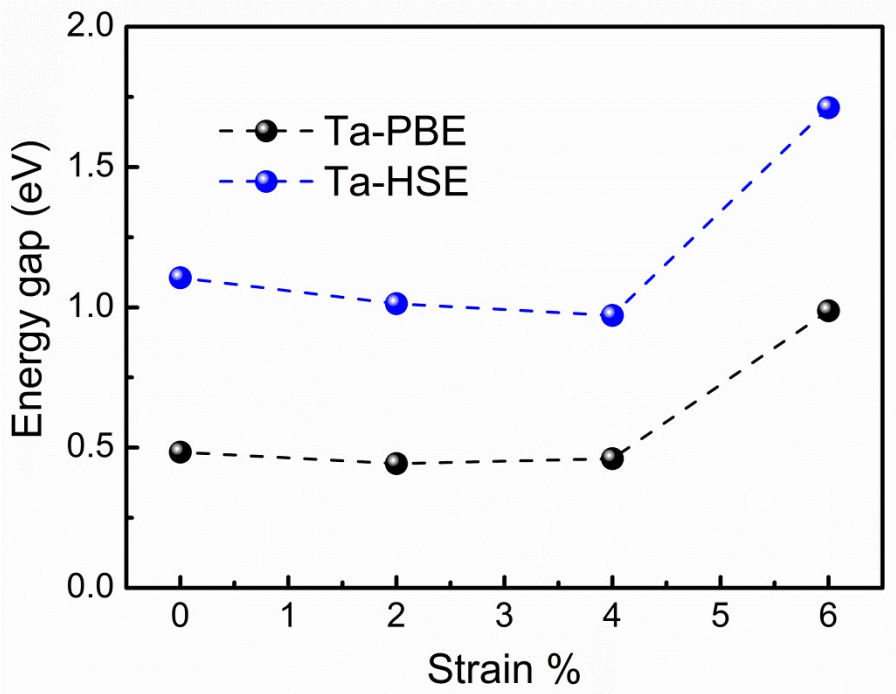

Fig. S14 The PBE/HSE band gap evolution of Ta_2CN_2 as a function of strain.

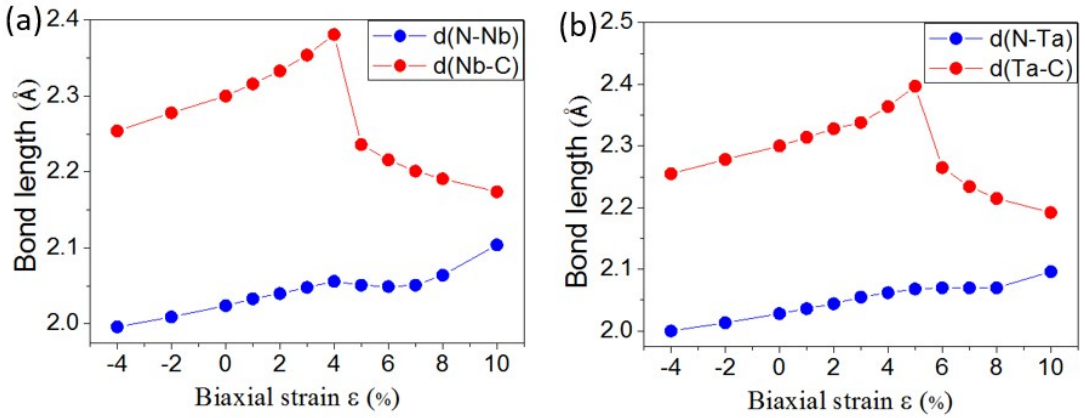

Fig. S15 The bond length evolution of Nb_2CN_2 (a) and Ta_2CN_2 (b) as a function of strain.

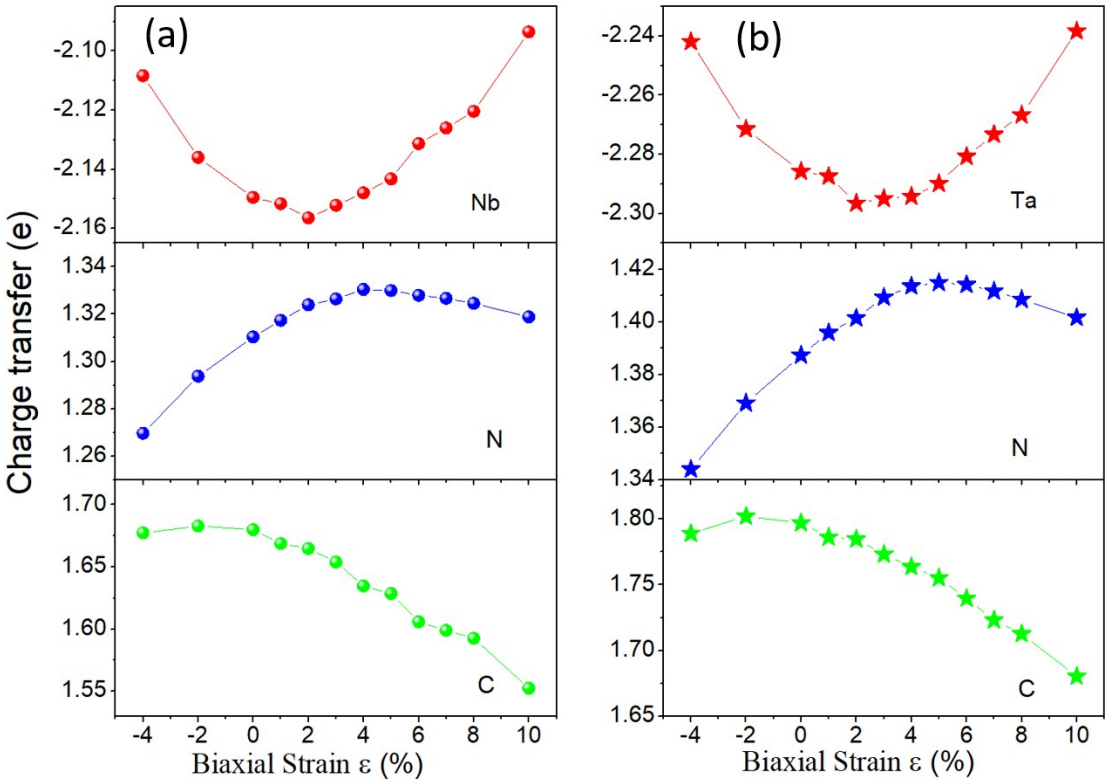

Fig. S16 The charge distribution of Nb_2CN_2 and Ta_2CN_2 as a function of strain.

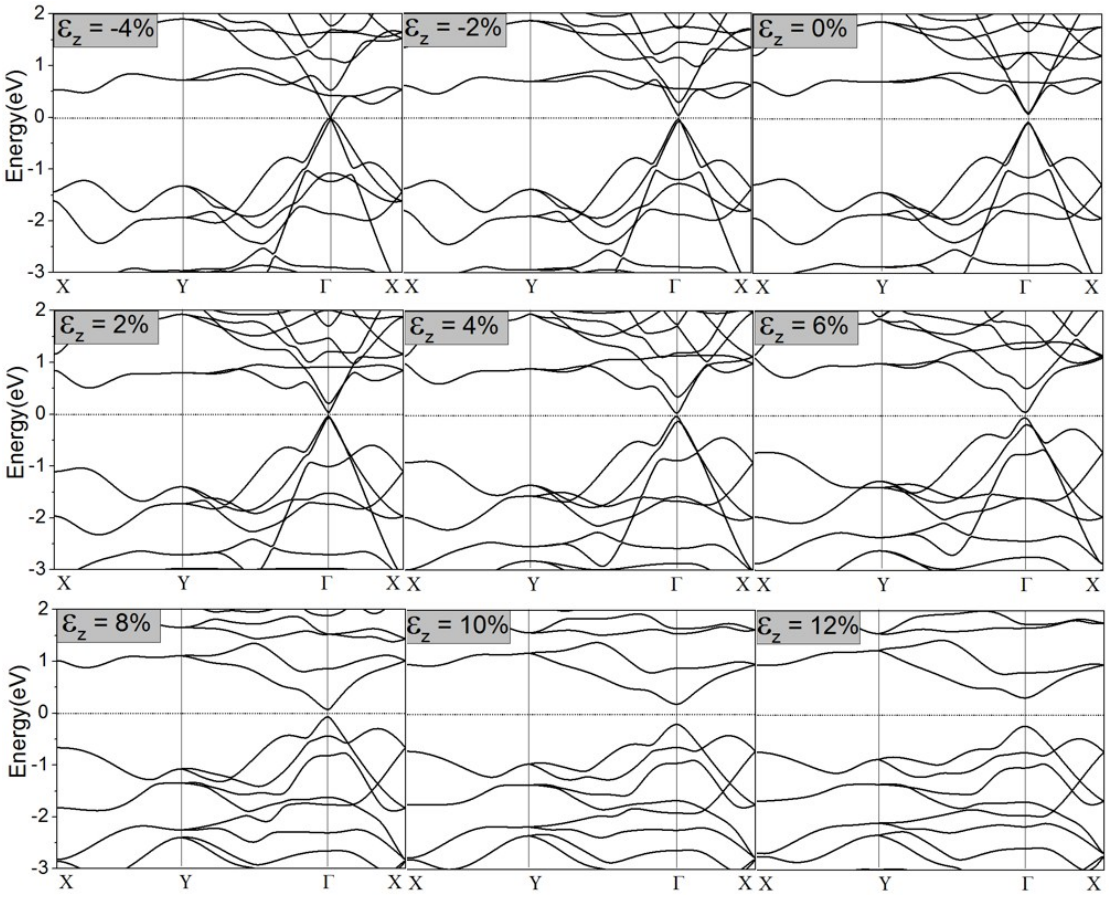

Fig. S17 The band structures of Nb_2CN_2 under various uniaxial strains along zigzag direction.

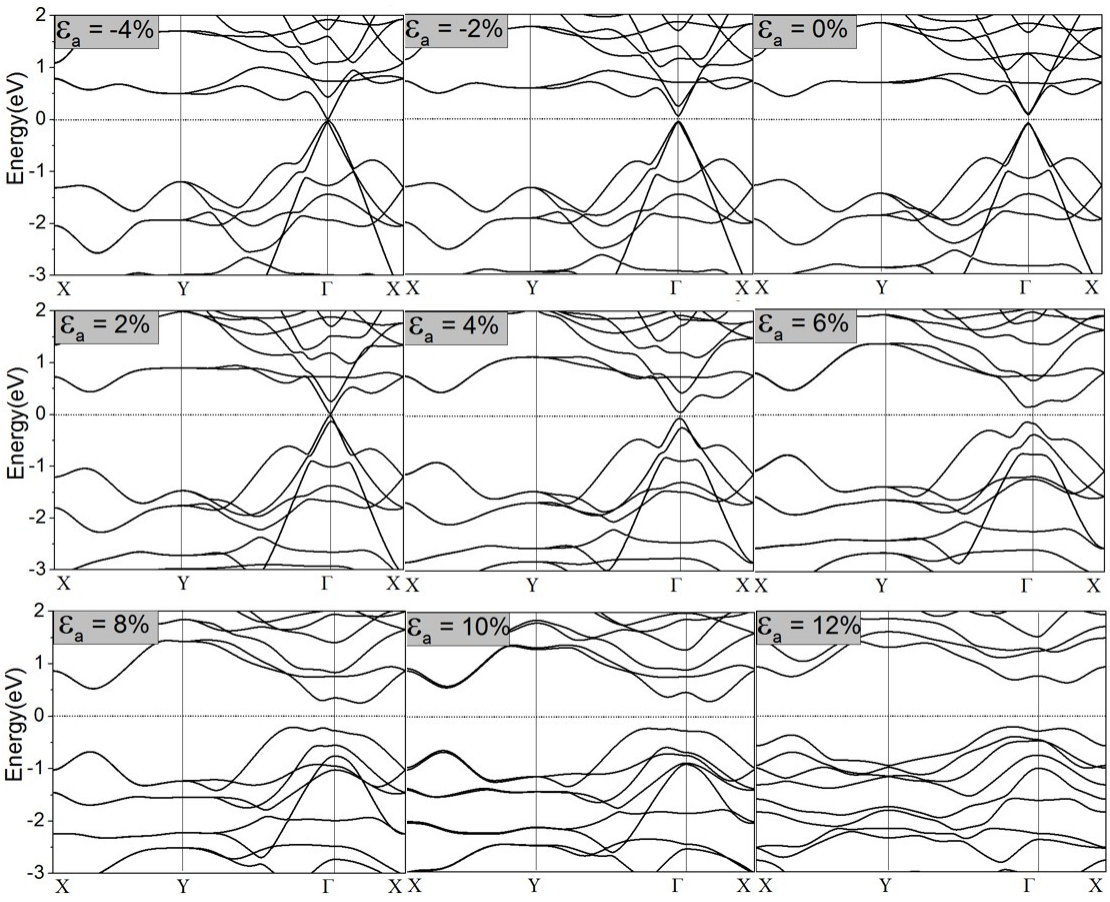

Fig. S18 The band structures of Nb_2CN_2 under various uniaxial strains along armchair direction.

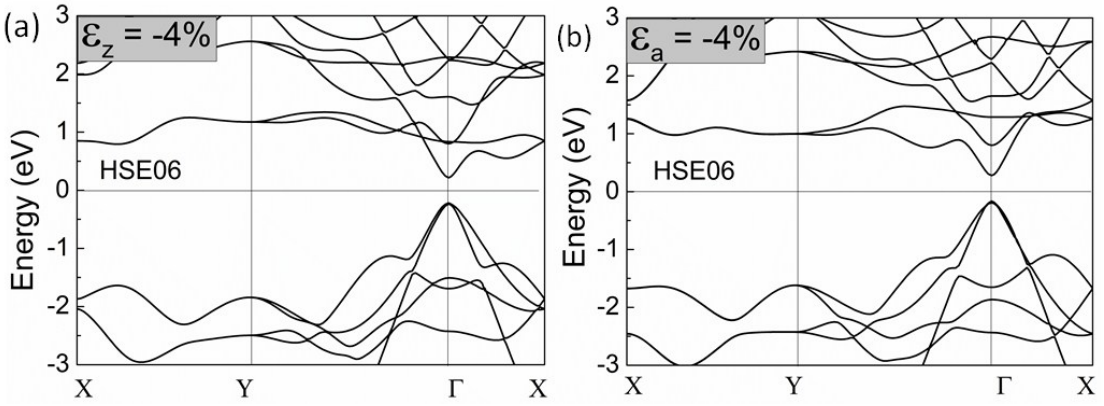

Fig. S19 Calculated HSE band structures at -4% uniaxial strain along zigzag (a) and armchair (b) directions, respectively.

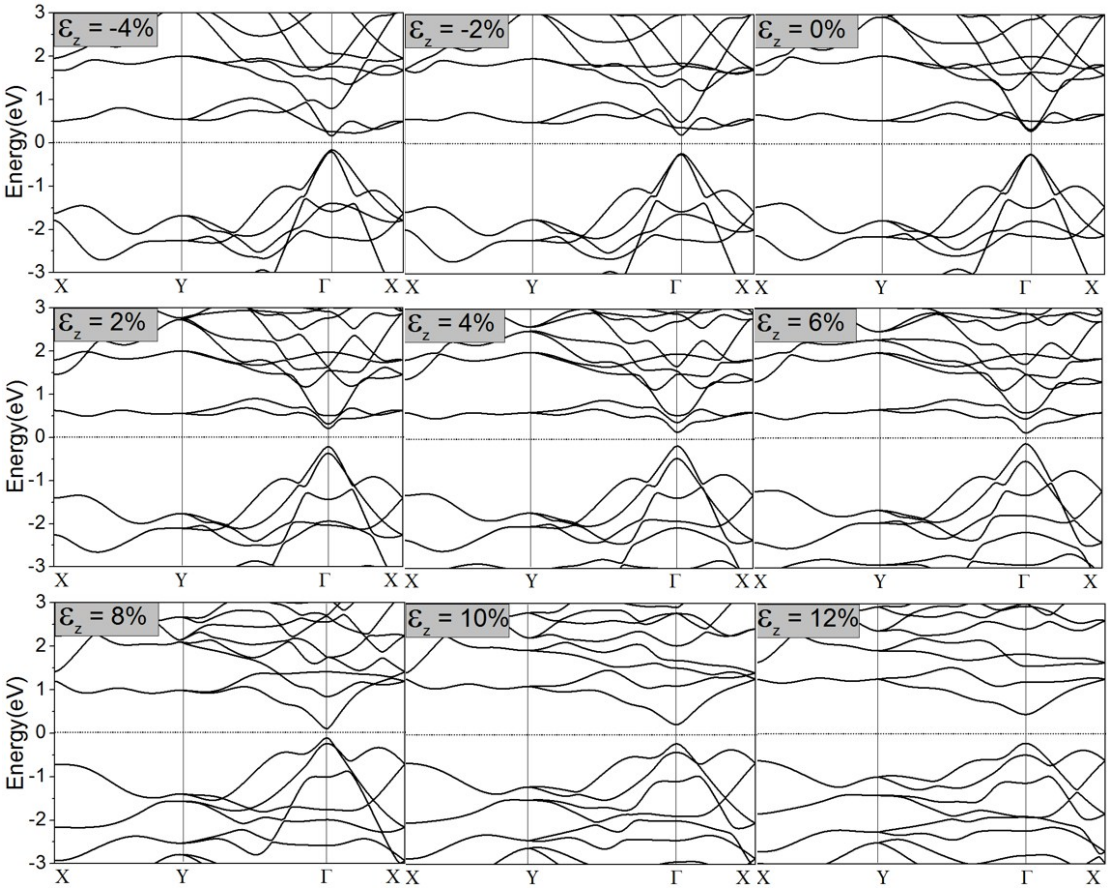

Fig. S20 The band structures of Ta_2CN_2 under various uniaxial strains along zigzag direction.

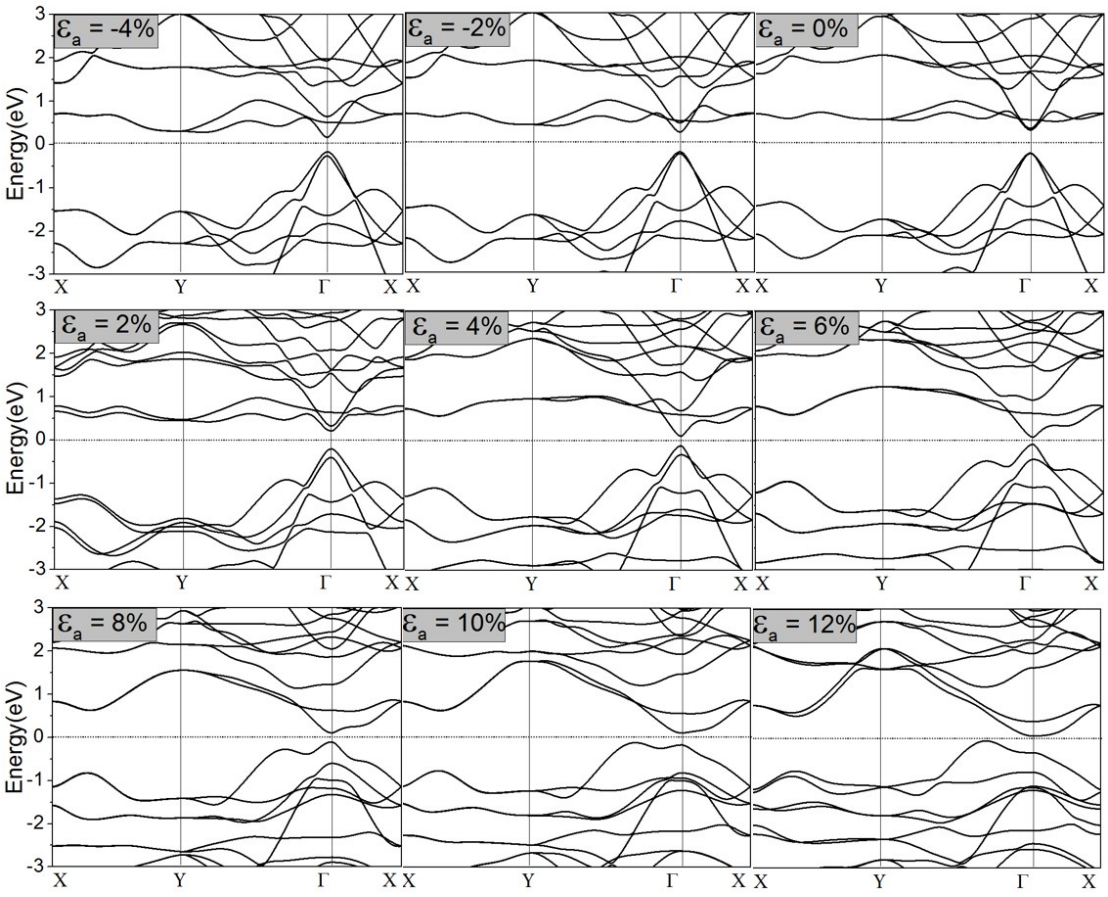

Fig. S21 The band structures of Ta_2CN_2 under various uniaxial strains along armchair direction.

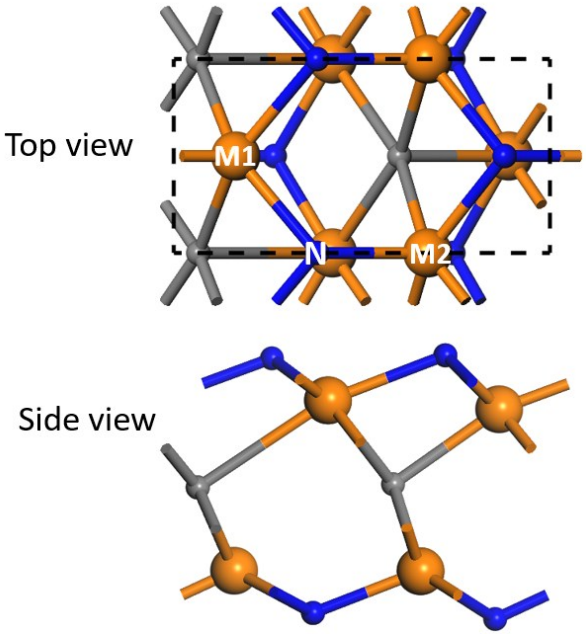

Fig. S22 Top view and side view of M_2CN_2 (M = Nb, &Ta) under uniaxial strain.

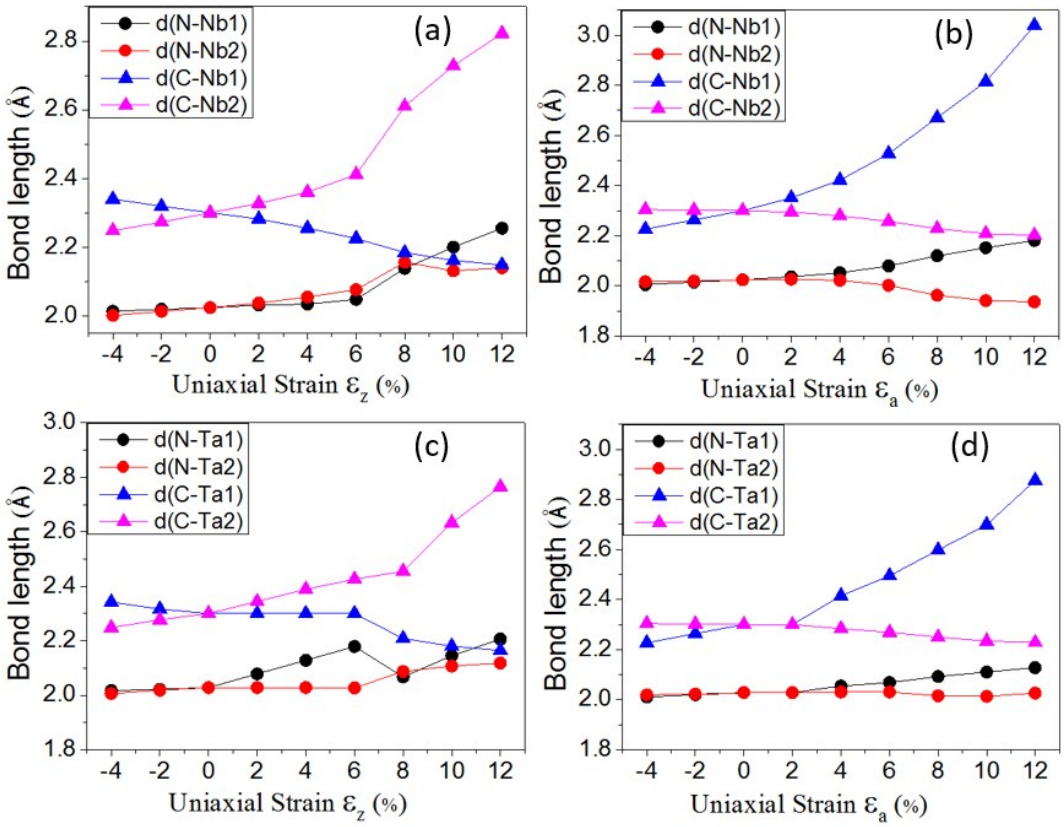

Fig. S23 The bond length evolution of Nb_2CN_2 (a) and Ta_2CN_2 (c) as a function of zigzag strain. The bond length evolution of Nb_2CN_2 (b) and Ta_2CN_2 (d) as a function of armchair strain.

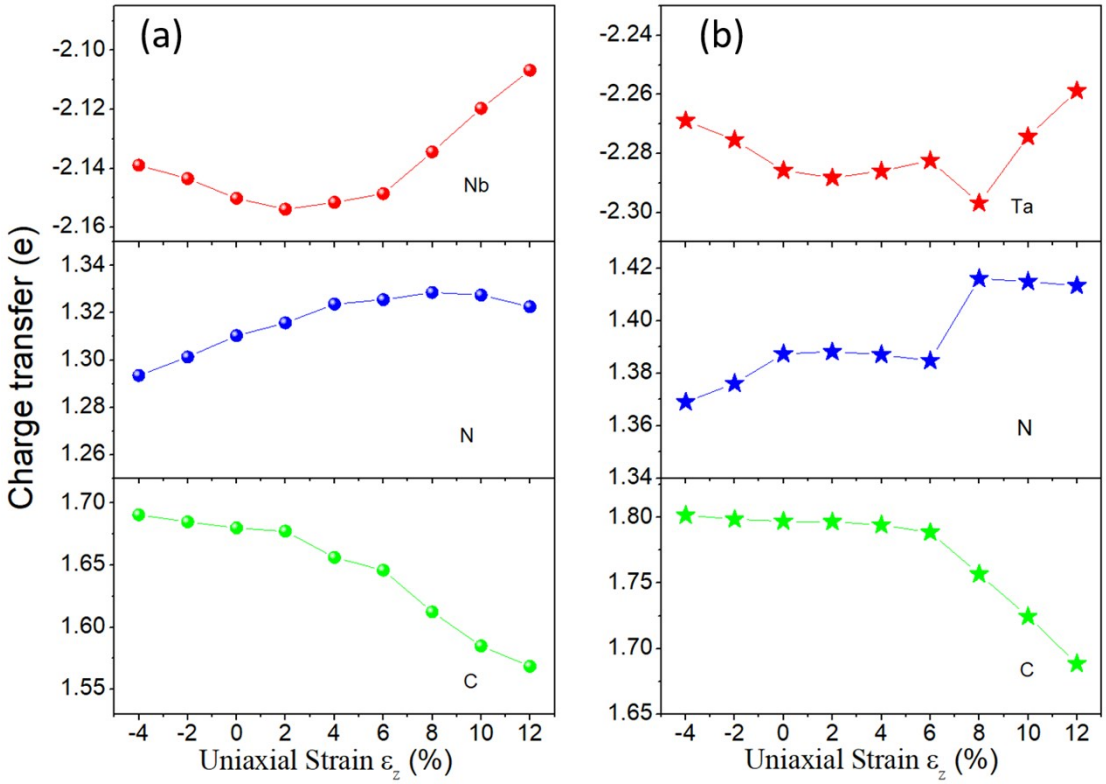

Fig. S24 The charge distribution of Nb_2CN_2 and Ta_2CN_2 as a function of zigzag strain.

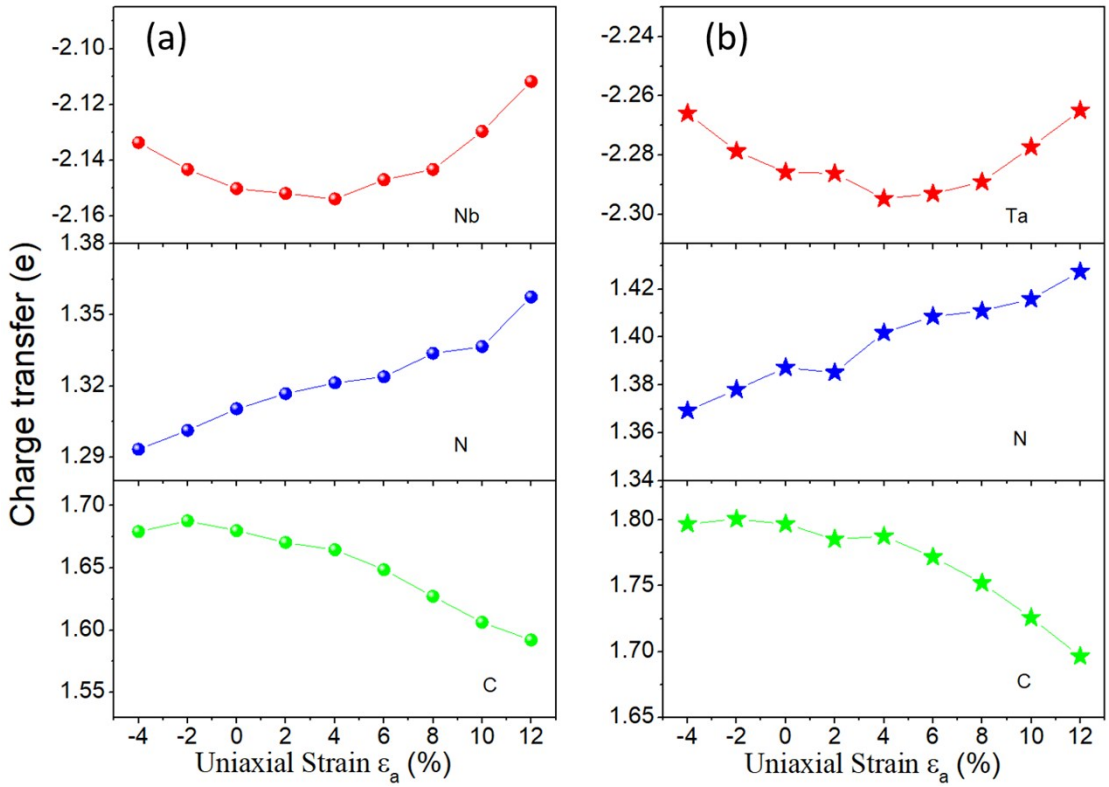

Fig. S25 The charge distribution of Nb_2CN_2 and Ta_2CN_2 as a function of armchair strain.

Structure data

Nb_2CN_2

1.00000000000000

3.1612999439000000 0.0000000000000000 0.0000000000000000

-1.5806499720000000 2.7377660603999998 0.0000000000000000

0.0000000000000000 0.0000000000000000 25.0000000000000000

N C Nb

2 1 2

Direct

0.3333300050000005 0.6666700239999983 0.5735399719999990

0.6666700239999983 0.3333300050000005 0.3915599879999974

0.0000000000000000 0.0000000000000000 0.4825499949999994

0.3333300050000005 0.6666700239999983 0.4265800120000023

0.6666700239999983 0.3333300050000005 0.5385100250000008

Ta_2CN_2

1.00000000000000

3.1603999138000001 0.0000000000000000 0.0000000000000000

-1.5801999569000000 2.7369866114999999 0.0000000000000000

0.0000000000000000 0.0000000000000000 25.0000000000000000

N C Ta

2 1 2

Direct

0.3333300050000005	0.6666700239999983	0.5585100050000023
0.6666700239999983	0.3333300050000005	0.3756699859999983
0.0000000000000000	0.0000000000000000	0.4670900110000034
0.3333300050000005	0.6666700239999983	0.4110800030000021
0.6666700239999983	0.3333300050000005	0.5231000189999975